THREE-DIMENSIONAL POROUS MEDIA MODEL OF A HORIZONTAL STEAM GENERATOR

T.J.H. Pättikangas, J. Niemi and V. Hovi

VTT Technical Research Centre of Finland, P.O.B. 1000, FI–02044 VTT, Finland

T. Toppila and T. Rämä

Fortum Nuclear Services Ltd, P.O.B. 100, FI–00048 FORTUM, Finland

Abstract

A three-dimensional porous media model has been implemented for the secondary side of the horizontal steam generator of a VVER-440 plant by using the ANSYS FLUENT 12.0 code. The primary circuit is solved with the APROS system code and the outer wall temperatures are interpolated to the CFD model. The necessary models for the heat and mass transfer and drag are implemented as User Defined Functions in the Euler-Euler two-phase model of the FLUENT code. The steady state full power operation of the steam generator is solved. The calculated result is compared to void fraction and flow velocity measurements at a few points. The shape of the surface level is compared to observations.

1. INTRODUCTION

In a steam generator of a pressurized water reactor (PWR), water is evaporated on the secondary side by the heat flux transported by the hot water on the primary side. The generated steam is conducted further to turbines to be transformed into mechanical energy and further to be used for the electricity production. Two types of PWR steam generators exist: the Western reactors include mostly vertical steam generators[1] but in VVER-type plants horizontal steam generators have been applied. Geometry of the horizontal VVER-440 steam generator is illustrated in Figure 1.

In horizontal steam generators, the heat transfer tubes are put horizontally into the water pool located in a horizontal cylindrical vessel. The mixture of water and steam is circulating in different flow patterns between the tubes and peripheral regimes. Between tubes the flow is mainly upwards directed two-phase flow, where steam is rising faster than water, but the most essential phase separation takes place in the open pool above the tube banks. The steam penetrates through the water level into the steam space, containing perhaps a small concentration of liquid as droplets. Steam dryers are located above the water level before the steam outlet leading into the steam lines.

The models for nucleate boiling of commercial computational fluid dynamics (CFD) codes are achieving the level, where it is possible to apply them for problems in nuclear power plants. Since the geometry of the steam generator is very complicated, only small part of the tubes could be modelled by using a detailed geometry model. Therefore, one has to use a simplified approach, where the tubes are not described in detail in the model of the secondary side of the steam generator. Instead the tubes are described with a porous media model, where the effect of the tubes on the two-phase flow is modelled by using pressure loss and source terms for enthalpy and mass.

In modelling the secondary side of the steam generator, it is important to use a realistic model for the primary circuit because it determines the boundary condition and the result of the calculation. Therefore, the APROS system code (APROS, 2009) is used for modelling the primary circuit and for the calculation of the source terms of enthalpy on the secondary side.

[1] Babcock&Wilcox once-through vertical steam generators could be considered as a third type.

In CFD modelling of the secondary side, the Euler-Euler multiphase model of the commercial ANSYS FLUENT 12.0 CFD code is used (ANSYS, 2009). In the Euler-Euler model, the equations for mass, momentum and enthalpy conservation are solved for two phases: liquid and vapour. The tubes of the primary circuit are described by using porous media model. The numerical model used in this work contains the relevant interactions between the phases, such as the drag forces and the mass transfer between the phases due to evaporation and condensation. The interactions between the phases have been implemented as User Defined Functions in FLUENT.

In this work, the basic equations needed for modelling a horizontal steam generator of a VVER-440 reactor are described. In writing the interaction terms of the phases, guidance has been taken from the work of Stosic and Stevanovic (2002) who have used a porous media model for modelling a steam generator of a VVER-1000 nuclear reactor. The experimental friction correlations for two-phase flow presented by Simovic et al. (2007) have been utilized. A somewhat similar approach to steam generator modelling has also been earlier used by Kristóf et al. (2008).

In Section 2, the basic conservation laws for mass, momentum and energy are formulated. Different drag forces affecting the vapour and liquid phases in the porous media model are discussed. Mass transfer between the phases due to evaporation and condensation is described. The source terms of the energy equation are formulated, which are related to phase changes and heat transfer. In Section 3, the APROS model of the primary circuit and the FLUENT model of the secondary side are described. Coupling of the APROS and FLUENT models is discussed. In Section 4, results on the validation calculations are presented. Finally, Section 5 summarizes the work and contains some discussion.

2. POROUS MEDIA MODEL

In the following, the basic conservation laws of mass, momentum and energy in the Euler-Euler multiphase model are formulated. The model equations are written in the form used in the ANSYS FLUENT version 12.0 and the source terms are formulated in the form suitable for implementation as User Defined Functions in FLUENT. Most of the time the approach presented earlier by Stosic and Stevanovic (2002) is followed.

2.1 Conservation Laws

Conservation of mass of phase q is (ANSYS, 2009)

$$\frac{\partial}{\partial t}(\gamma\alpha_q\rho_q) + \nabla\cdot(\gamma\alpha_q\rho_q\mathbf{v}_q) = S_{\text{mass},q} \tag{1}$$

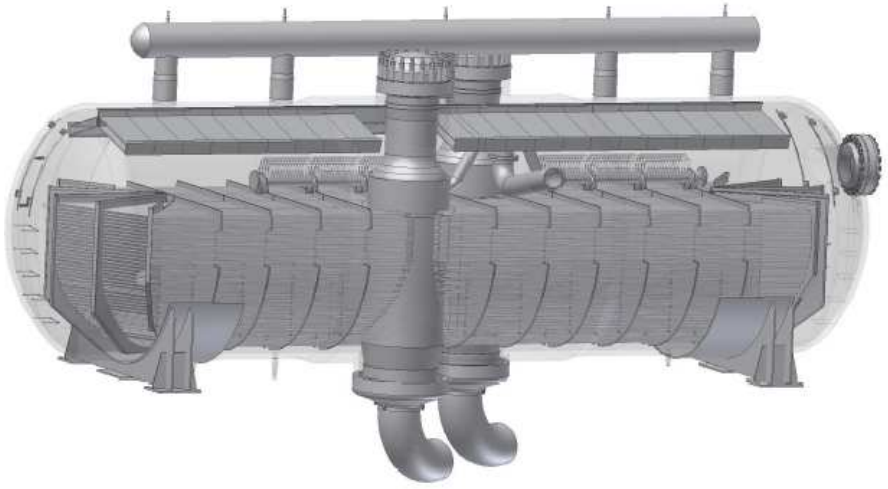

Fig. 1: Horizontal steam generator of a VVER-440 plant.

where γ is porosity, α_q is the volume fraction, ρ_q is the density and $\mathbf{v}_q$ is the velocity of phase q. The index q = 1 stands for the liquid phase and q = 2 for the vapour phase. The sum of the volume fractions is $\alpha_1 + \alpha_2 = 1$. Evaporation and condensation are described with the source term $S_{\text{mass},q}$.

Conservation of momentum of phase q is

$$\frac{\partial}{\partial t}(\gamma\alpha_q\rho_q\mathbf{v}_q) + \nabla\cdot(\gamma\alpha_q\rho_q\mathbf{v}_q\mathbf{v}_q) = \mathbf{S}_{\text{M},q} \tag{2}$$

The source term $\mathbf{S}_{\text{M},q}$ on the right-hand side contains interphase momentum transfer, lift force and virtual mass force. In addition, it includes effects of pressure gradient, gravitation and turbulence.

Conservation of energy is

$$\frac{\partial}{\partial t}(\gamma\alpha_q\rho_q h_q) + \nabla\cdot(\gamma\alpha_q\rho_q\mathbf{v}_q h_q) = S_{\text{E},q} \tag{3}$$

where h_q is the specific enthalpy of the phase q. The source term $S_{\text{E},q}$ on the right-hand side includes the interfacial heat exchange and the heat source from the porous media, i.e., the tube banks. In addition, it contains effects of turbulence and changing pressure.

2.2 Momentum Source Terms

In the conservation law of momentum, Eq. (2), the source term is (ANSYS, 2009)

$$\mathbf{S}_{\text{M},q} = -\gamma\alpha_q\nabla p + \nabla\cdot\left(\gamma\boldsymbol{\tau}_q\right) + \gamma\alpha_q\rho_q\mathbf{g} + \mathbf{R}_{pq} + \mathbf{F}_{\text{CE},q} + \mathbf{F}_{\text{lift},q} + \mathbf{F}_{\text{vm},q} + \mathbf{F}_{\text{DF},q} \tag{4}$$

where p is the pressure and $\mathbf{g}$ is the gravitational acceleration. The stress-strain tensor is denoted by $\boldsymbol{\tau}_q$ and $\mathbf{R}_{pq}$ is the interfacial friction force and $\mathbf{F}_{\text{DF},q}$ is the friction caused by the tubes of the primary circuit. $\mathbf{F}_{\text{CE},q}$ is the force related to momentum transfer between phases, when mass transfer between phases occurs. $\mathbf{F}_{\text{lift},q}$ is the lift force and $\mathbf{F}_{\text{vm},q}$ is the virtual mass force. The main forces driving the flow are the gravitational forces, wall friction affecting both phases and the interfacial friction.

The interfacial drag force

The interfacial drag force is proportional to the velocity difference between the phases:

$$\mathbf{R}_{21} = K_{21}(\mathbf{v}_2 - \mathbf{v}_1) \tag{5}$$

The interfacial momentum exchange coefficient, K_{21}, is

$$K_{21} = \frac{3}{4}\alpha_2\rho_1\frac{C_{\text{D}}}{d_2}\left|\mathbf{v}_2 - \mathbf{v}_1\right| \tag{6}$$

The correlation for the ratio of interfacial drag coefficient and the bubble diameter, C_{D}/d_2, consists of three parts described below.

The first part, which is valid for bubbly flow regime ($\alpha_2 < 0.3$), has been adopted from Ishii and Zuber (1979). Stosic and Stevanovic (2002) have modified the original correlation by multiplying it by 0.4. This made a better fit to their experimental data, which was bubbly flow over a horizontal tube bank:

$$\frac{C_{\text{D}}}{d_2} = 0.267\left(\frac{g\Delta\rho}{\sigma}\right)^{1/2}\left[\frac{1+17.67\,f(\alpha_2)^{6/7}}{18.67\,f(\alpha_2)}\right]^2 \tag{7}$$

Here g is the acceleration of gravity, $\Delta\rho$ is the difference between liquid and vapour density, σ is the surface tension, and the dependence on the void fraction is $f(\alpha_2) = (1-\alpha_2)^{3/2}$. The second part of the correlation for churn-turbulent flows ($\alpha_2 > 0.3$) reads as

$$\frac{C_{\mathrm{D}}}{d_2} = 1.487\left(\frac{g\Delta\rho}{\sigma}\right)^{1/2}(1-\alpha_2)^3(1-0.75\alpha_2)^2 \tag{8}$$

where the dependence on void fraction has the same form as in the CATHARE code. The third part of the correlation is valid for annular and mist flow ($\alpha_2 > 0.3$)

$$\frac{C_{\mathrm{D}}}{d_2} = 7.136\times10^{-5}\left(\frac{g\Delta\rho}{\sigma}\right)^{1/2}(1-\alpha_2)\left|\mathbf{v}_2\right|^2 \tag{9}$$

The larger value of the second and third parts of the correlation is selected.

Drag force caused by the tubes of the primary circuit

On the secondary side, the pressure losses caused by the tubes of the primary circuit are described based on the porous material formulation. The pressure loss is divided between the phases as $\mathbf{F}_{\mathrm{DF},q} = \gamma\alpha_q\mathbf{F}_{\mathrm{DF}}$, where

$$\mathbf{F}_{\mathrm{DF}} = -\sum_p \alpha_p\mu_p\mathbf{D}_p\mathbf{v}_p - \frac{1}{2}\sum_p \alpha_p\rho_p\left|\mathbf{v}_p\right|\mathbf{C}_p\mathbf{v}_p \tag{10}$$

In the porous media approximation, the drag forces on the fluid phases consist of two parts: a viscous loss term proportional to flow velocity and an inertial loss term proportional to the square of the flow velocity. In an anisotropic porous medium, such as the tube banks, the proportionality coefficients describing the friction forces, $\mathbf{D}_p$ and $\mathbf{C}_p$, are tensors. The effect of the viscous loss term has been ignored, $\mathbf{D}_p = 0$, because the proportionality coefficient describing the inertial loss term, $\mathbf{C}_p$, becomes dominant when flow velocities are large; $\mathbf{C}_p$ is also assumed to be diagonal.

The pressure losses in the cross flow direction and in the direction parallel to the tubes are

$$F_{\mathrm{DF},\perp} = -\frac{1}{2}\sum_p \alpha_p\rho_p C_{p,\perp}\left|\mathbf{v}_p\right|v_{p,\perp} \tag{11}$$

$$F_{\mathrm{DF},\parallel} = -\frac{1}{2}\sum_p \alpha_p\rho_p C_{p,\parallel}\left|\mathbf{v}_p\right|v_{p,\parallel} \tag{12}$$

In the direction parallel to the tubes, the Blasius correlation is applied $C_{p,\parallel} = 0.3165/(D_{\mathrm{e}}\,\mathrm{Re}_p^{0.25})$, where D_{e} is the equivalent diameter and Re_p is Reynolds number of phase p.

In the cross-flow direction, the pressure loss is calculated according to the model presented by Simovic et al. (2007). The pressure loss coefficient for equilateral in-line tube arrangement is $C_{p,\perp} = 2\mathrm{Eu}_p / P$, where P is the equilateral pitch. The phasic Euler numbers are

$$\mathrm{Eu}_p = 0.265\left[\left(\frac{P}{d_3}-0.8\right)\Big/\left(\frac{P}{d_3}-1\right)\right]^n \mathrm{Re}_p^m \tag{13}$$

where d_3 is the outer diameter of the tubes and Re_p is the Reynolds number for phase p. The exponents m and n are calculated as has been described by Simovic et al. (2007).

2.3 Mass Source Terms

The mass transfer between the phases is included as a source term in the continuity equation, Eq. (1), for each phase. The source term for the liquid phase caused by condensation of vapour and evaporation of liquid is

$$S_{\text{mass},1} = \dot{m}_{21} - \dot{m}_{12} + \dot{m}_{21,\text{PR}} - \dot{m}_{12,\text{PR}} \tag{14}$$

The mass transfer rate from the phase *p* to the phase *q* due to bulk evaporation and/or condensation is $\dot{m}_{pq}$. The mass transfer rate from phase *p* to phase *q* due to the heat transferred from the primary circuit is $\dot{m}_{pq,\text{PR}}$, which is discussed in detail in Sec. 2.4. The source term for the continuation equation of the vapour phase is $S_{\text{mass},2} = -S_{\text{mass},1}$.

Evaporation occurs, when the liquid enthalpy is higher than the liquid saturation enthalpy, i.e., $h_1 > h'$, whereas condensation occurs, when vapour is in contact with subcooled liquid, i.e., $h_1 < h'$. The bulk evaporation and condensation are calculated from the correlations

$$\begin{aligned} &\text{evaporation :} \quad \dot{m}_{12} = \frac{\alpha_1 \rho_1}{\tau_\text{e}} \frac{h' - h_1}{h'' - h'} \\ &\text{condensation :} \quad \dot{m}_{21} = \frac{\alpha_1 \rho_1}{\tau_\text{c}} \frac{h_1 - h'}{h'' - h'} \end{aligned} \tag{15}$$

where τ_e is the evaporation relaxation time and τ_c is the condensation relaxation time. Constant values of one second have been adopted for both relaxation times.

2.4 Energy Source Terms

In the conservation law of energy, Eq. (3), the source term is (ANSYS, 2009)

$$S_{\text{E},q} = -\gamma \alpha_q \frac{\partial p}{\partial t} + \gamma \boldsymbol{\tau}_q : \nabla \mathbf{v}_q - \nabla \cdot \left(\gamma \mathbf{q}_q \right) + Q_{pq} + S_{\text{EC},q} + S_{\text{PR},q} \tag{16}$$

where $\mathbf{q}_q$ is the heat flux, Q_{pq} is the intensity of heat exchange between phases *p* and *q*. The last two terms are related to bulk condensation and evaporation and to heat transfer from the primary circuit.

The source term of enthalpy caused by the bulk evaporation and condensation is for the liquid phase

$$S_{\text{EC},1} = (\dot{m}_{21} - \dot{m}_{12})(h'' - h_1) \tag{17}$$

The corresponding source term in the enthalpy equation for vapour is $S_{\text{EC},2} = -S_{\text{EC},1}$.

In the following, the heat transfer from the primary circuit to the secondary side is written in the porous media formulation. The volumetric heat transfer rate for the liquid heating is

$$q'''_{\text{w},1} = h''_{\text{w},1} (T_\text{w} - T_1)(A_\text{s} / V_\text{tot}) (1 - \alpha_2) \tag{18}$$

where the surface related heat transfer coefficient is calculated from the Dittus-Boelter correlation:

$$h''_{\text{w},1} = 0.023 (\lambda_1 / D_\text{e}) \, \text{Re}_\text{m}^{0.8} \, \text{Pr}_1^{0.4} \tag{19}$$

The Reynolds number for the mixture is defined as $\text{Re}_\text{m} = \rho_\text{m} |\mathbf{v}_\text{m}| D_\text{e} / \mu_1$, where the mixture density and velocity are defined as volume averaged quantities. The equivalent diameter for the complex tube bank is derived from the fluid volume and surface area as $D_\text{e} = 4 V_\text{f} / A_\text{s}$.

When the heating walls are in contact with vapour, the heat transfer rate is

$$q'''_{\text{w},2} = h''_{\text{w},2} (T_\text{w} - T_2)(A_\text{s} / V_\text{tot}) \alpha_2 \tag{20}$$

where $h''_{\text{w},2}$ is obtained from the Dittus-Boelter correlation: $h''_{\text{w},2} = 0.023 (\lambda_2 / D_\text{e}) \, \text{Re}_\text{m}^{0.8} \, \text{Pr}_2^{0.4}$.

Boiling is added to the heat transfer, when the structure temperature exceeds the saturation temperature. The volumetric boiling correlation reads

$$q'''_{\mathrm{wb}} = h''_{\mathrm{wb}} \max(T_{\mathrm{w}} - T_{\mathrm{sat}}, 0)(A_{\mathrm{s}} / V_{\mathrm{tot}})(1-\alpha_2)^{0.1} \tag{21}$$

where the Thom pool boiling correlation is used for the surface area heat transfer coefficient

$$h''_{\mathrm{wb}} = 1971.2\, e^{0.023p}(T_{\mathrm{w}} - T_{\mathrm{sat}}) \qquad [h''_{\mathrm{wb}}] = \mathrm{W/m^2K} \tag{22}$$

An additional limiter, $(1-\alpha_2)^{0.1}$, has been included to limit the heat transfer at high void fractions.

When the liquid sub-cooling exceeds T_{R} = 20 K, all the heat transferred from the primary circuit is used in liquid heating. For saturated and superheated liquid, all the heat transferred from the primary circuit is used for steam generation. Between these two limiting cases, linear interpolation is used for dividing the heat between liquid heating and steam generation. The volumetric steam generation is

$$\dot{m}_{12,\mathrm{PR}} = (1-r)(q'''_{\mathrm{wb}} + q'''_{\mathrm{w},1}) / h_{\mathrm{fg}} \tag{23}$$

where the linear ramp function is defined as $r = \min[\max((T_{\mathrm{sat}} - T_1)/T_{\mathrm{R}}, 0), 1]$. The corresponding energy source term for vapour is

$$S_{\mathrm{PR},2} = \dot{m}_{12,\mathrm{PR}} h_{\mathrm{fg}} + q'''_{\mathrm{w},2} \tag{24}$$

The rest of the total heat flux is used for liquid heating

$$S_{\mathrm{PR},1} = r(q'''_{\mathrm{wb}} + q'''_{\mathrm{w},1}) \tag{25}$$

3. THREE-DIMENSIONAL MODEL OF A VVER-440 STEAM GENERATOR

The horizontal steam generator of a VVER-440 PWR is first modelled by using the APROS code. The outer wall temperatures of the tubes of the primary circuit are calculated and then used as an input to the FLUENT model of the secondary side. In the following, the APROS and the FLUENT models are presented and the APROS-FLUENT coupling is briefly described.

In the APROS model, the primary circuit has been divided into five horizontal layers. The uppermost layer is presented in Fig. 2. Several tubes are modelled with the same APROS component: four consecutive tubes in the horizontal direction and fifteen in the vertical direction. The flow rate of the primary circuit is controlled by a control valve and a control circuit.

The secondary side of the steam generator is presented in Fig. 3. The portion of the secondary side occupied by the tube banks has also been divided into five horizontal layers. Five vertically aligned "downcomer" nodes have been added to allow some recirculation, and the area above the tube banks (steam dome) is modelled with two nodes. The heat transferred in each of the five layers of the primary circuit is conveyed into its own node on the secondary side. The feed water flow is adjusted with a three-point control, which monitors the water level of the uppermost downcomer node.

The secondary side of the horizontal steam generator has been modelled by using the Euler-Euler multiphase model of FLUENT 12.0. The portion of the steam generator occupied by the tube banks has been described with the porous media model of FLUENT, which introduces additional source terms for the pressure loss caused by the tube banks and the enthalpy source. The source terms described in Section 2 were implemented as User Defined Functions in the FLUENT model.

Most of the simulations were performed with a FLUENT model consisting of 120 000 grid cells. The grid independency was checked by performing a few simulations with mesh consisting of about 950 000 grid cells. The grid is almost purely hexahedral. The free flow areas are modelled with a finer mesh than the porous areas. The tube support plates are represented as thin walls. The inner structures of the FLUENT model are illustrated in Fig. 4, where the tube banks are shown in green and the support plates and collectors are shown in brown. The new feed water manifold can be seen above the tube banks on the hot side. The old feed water manifold is located in the middle of the tube banks.

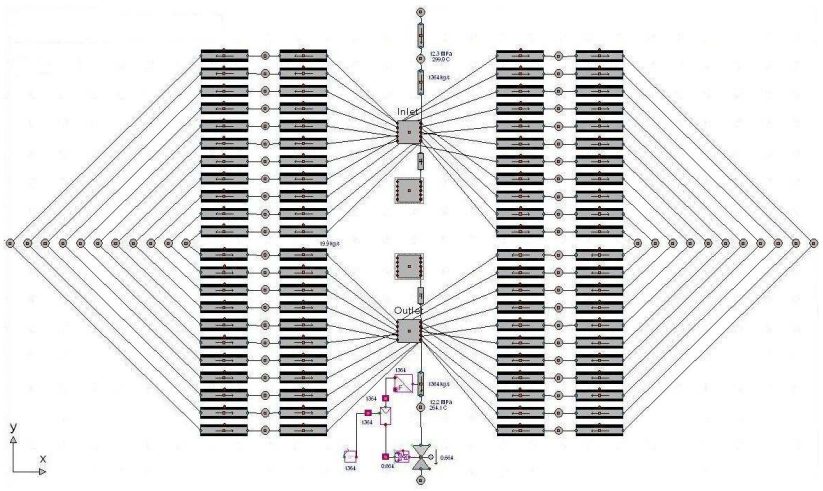

Fig. 2: The uppermost level of the primary circuit in the APROS model of the VVER-440 horizontal steam generator.

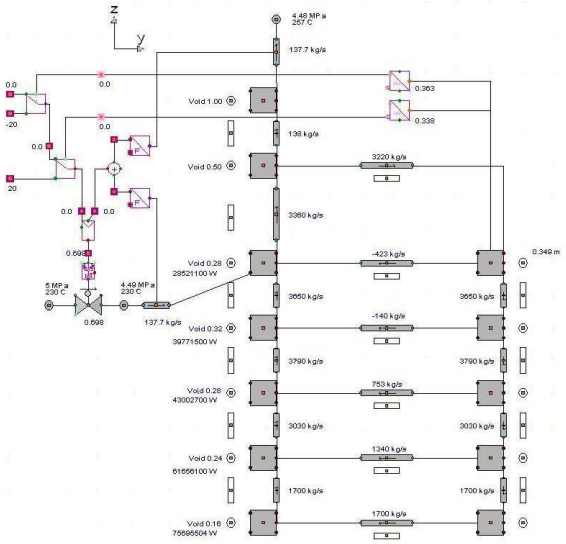

Fig. 3: The secondary side of the APROS model for the VVER-440 steam generator.

In the spatial discretization, the QUICK scheme was used for the volume fraction and the second order upwind scheme for other quantities. For the pressure-velocity coupling, the phase coupled SIMPLE scheme was used. In the temporal discretization, the first order implicit method was used with a time step of Δt = 0.05 s for the coarse mesh. The primary tubes were modelled as porous media with a porosity of 0.72. Turbulence was modelled with the k-ε turbulence model for the mixture of liquid and vapour. The effect of the primary tubes on the turbulence on the secondary side was not taken into account in the model.

Simulation of the primary circuit by using APROS makes it possible to provide a realistic boundary condition for the CFD simulation of the secondary side. The temperatures of the outer walls of the tubes of the primary circuit are solved by using the APROS model. The wall temperatures are then interpolated from the nodes of the APROS model to each grid cell in the tube banks of the FLUENT model. The interpolation is based on finding the nearest APROS node for each grid cell of the FLUENT model. The outer wall temperatures are then used in the CFD simulation for calculation of the heat transfer from the primary circuit to the secondary side.

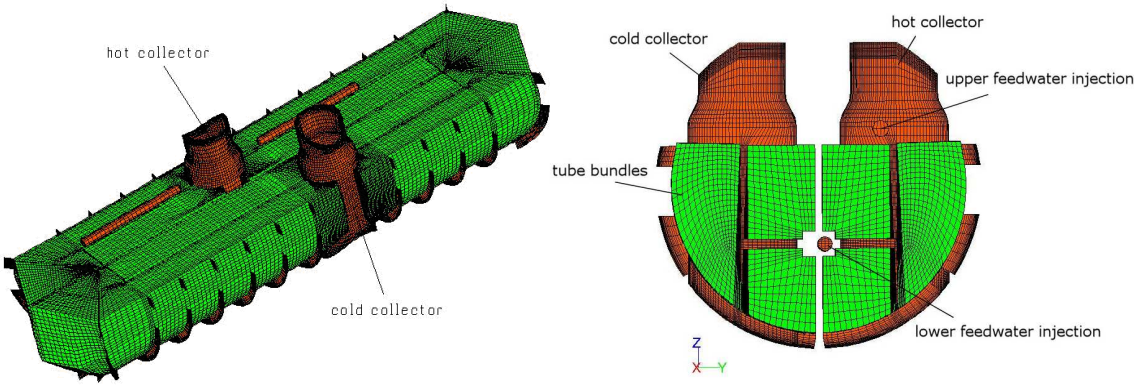

Fig. 4: The FLUENT model for the secondary side of the VVER-440 steam generator.

The flow on the secondary side is driven by gravitation and the density differences of the water-vapour mixture. The density differences are caused by the differences in void fraction, which are caused by differences in heat transfer on the cold and hot sides of the steam generator. Therefore, it is expected that the use of an accurate estimate for the wall temperatures of the primary circuit is a crucial step in determining the correct flow field on the secondary side.

4. SIMULATION OF THE VVER-440 STEAM GENERATOR

In the following, the steady state operation of the steam generator at full power is studied. In the simulations, the feed water was injected from the old feed water manifold located in the middle of the tube banks. The reason for this is that some measured data on void fractions is available for such a situation (Haapalehto and Bestion, 1993).

The parameters for VVER-440 steam generator are shown in Table 1, when the old feed water manifold is used. The mass of water on the secondary side was 33 tons in the stationary state that was the target. The temperature of the feed water was 223 °C and the injection rate was 130 kg/s. This corresponds to the full power of 242 MW of the steam generator. The steam generator is approximately 12 m long, and has a diameter of approximately 3 m. The heat transfer area is 2 510 m^2.

4.1 Simulation of the Stationary State

First, the temperatures of the primary tubes are solved with the APROS model. In Fig. 5, the outer wall temperatures of the tubes are shown, when the APROS result has been interpolated to the CFD mesh. Cooling down of the primary flow from the hot collector to the cold collector can be seen in the result. The temperature distribution is clearly three-dimensional. In addition to the difference between the hot and the cold side, the temperature also varies in the vertical direction. The tubes near the bottom are colder than those near the top of the tube banks.

In Fig. 6, the volumetric vapour generation rate is shown on the secondary side. As can be expected, the maximum amount of vapour is produced near the hot collector. Near the cold collector the vapour generation rate is very small. More vapour is generated in the top part of the tube banks than in the bottom.

In Fig. 7, the void fraction is shown in two vertical cross-sections of the steam generator. The position of the feed water manifold is indicated in the middle of the tube banks. Most of the feed water is injected towards the hot side, which can be clearly seen in the void fraction distribution. The surface level is higher on the hot side, where more steam is generated than on the cold side. Near the bottom, the void fraction is almost zero.

Table 1: Model parameters for the primary and the secondary side of the VVER-440 steam generator.

Primary side	
Inflow temperature of primary water, $T_{prim,in}$	295 °C
Outflow temperature of primary water, $T_{prim,out}$	265.7 °C
Mass flow rate of primary water, $\dot{m}_{prim}$	1 560 kg/s
Pressure, p_{prim}	122.5 bar

Secondary side	
Power	242 MW
Steam production	130.1 kg/s
Mass of water, m_{sec}	33 000 kg
Pressure, p_{sec}	46.0 bar
Temperature, T_{sat}	259 °C
Feed water injection	130.1 kg/s
Feed water temperature	222.9 °C

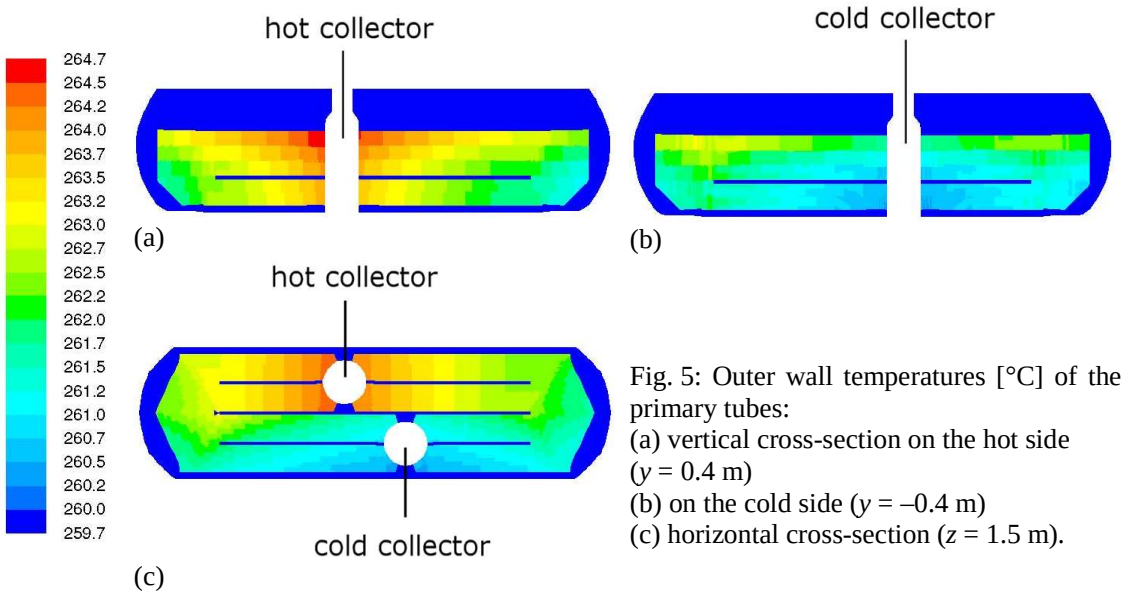

Fig. 5: Outer wall temperatures [°C] of the primary tubes:
(a) vertical cross-section on the hot side (y = 0.4 m)
(b) on the cold side (y = –0.4 m)
(c) horizontal cross-section (z = 1.5 m).

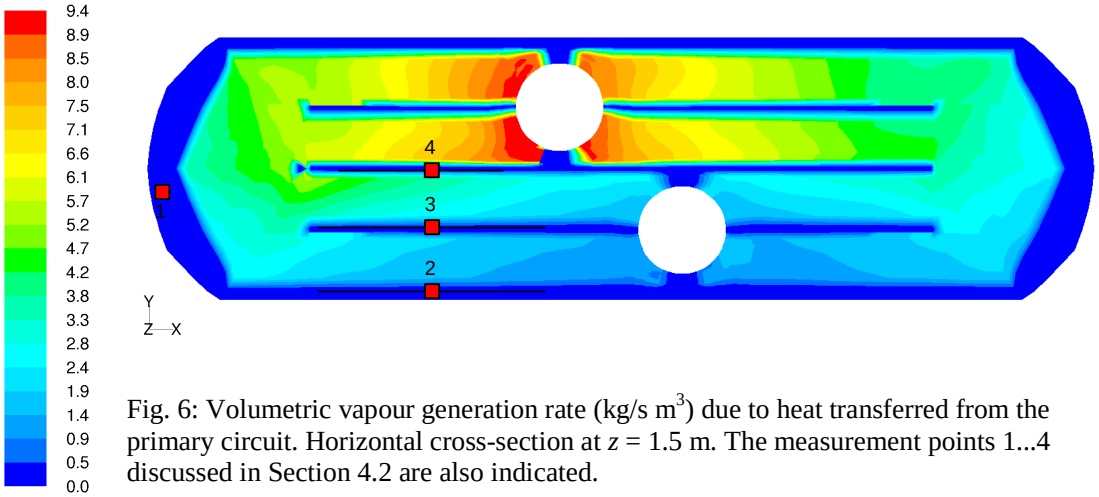

Fig. 6: Volumetric vapour generation rate (kg/s m^3) due to heat transferred from the primary circuit. Horizontal cross-section at z = 1.5 m. The measurement points 1...4 discussed in Section 4.2 are also indicated.

In Fig. 8, the void fraction is shown at the centre and in the hot end of the steam generator. The hot side is located on the right-hand side in these cross-sections. The bulk condensation caused by the cold feed water injected towards the hot side is clearly visible. In the bottom, the void fraction is smaller on the cold side than on the hot side.

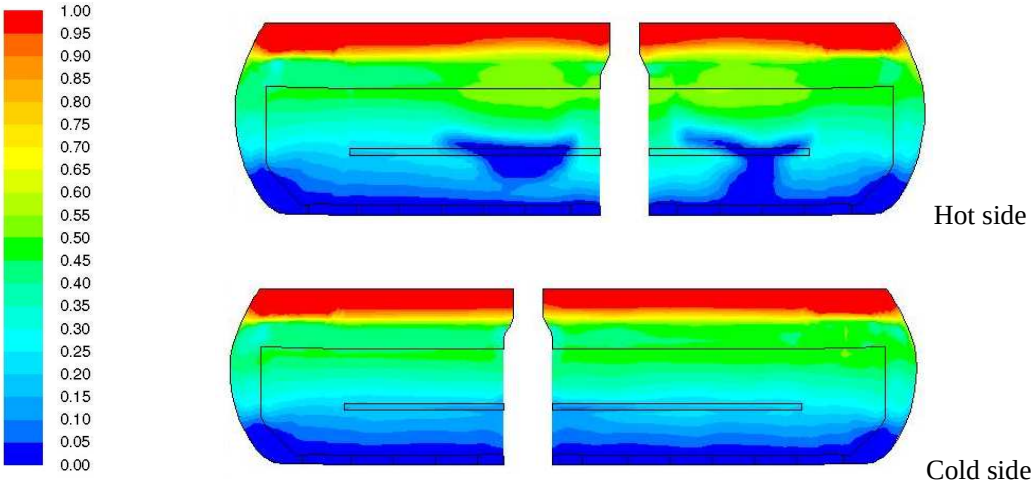

Fig. 7: Void fraction in the vertical cross-sections on the hot (y = 0.4 m) and cold side (y = –0.4 m).

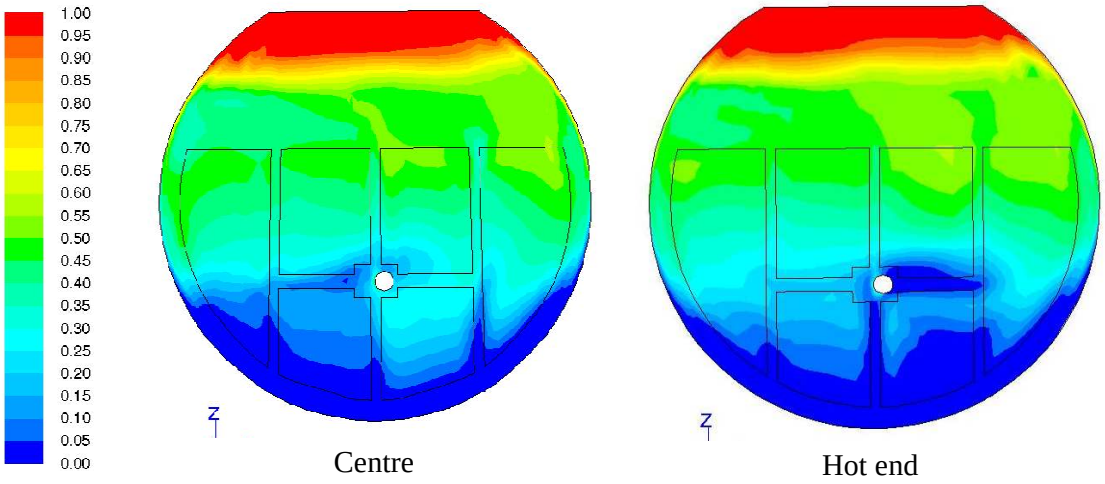

Fig. 8: Void fraction in vertical cross-sections at the centre (x = 0) and in the hot end (x = –2.67 m).

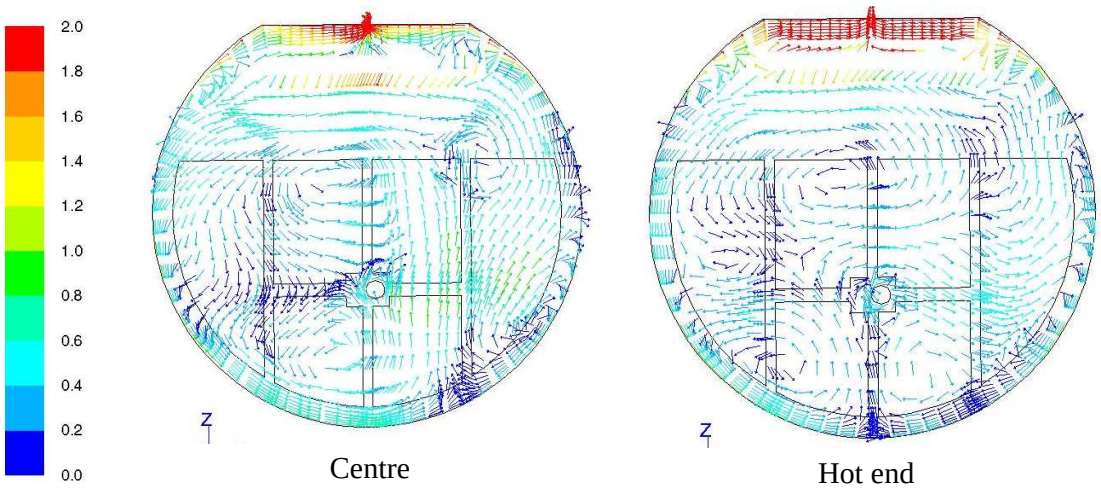

Fig. 9: Velocity magnitude of liquid water (m/s) in the vertical cross-sections at the centre (x = 0) and in the hot end (x = –2.67 m).

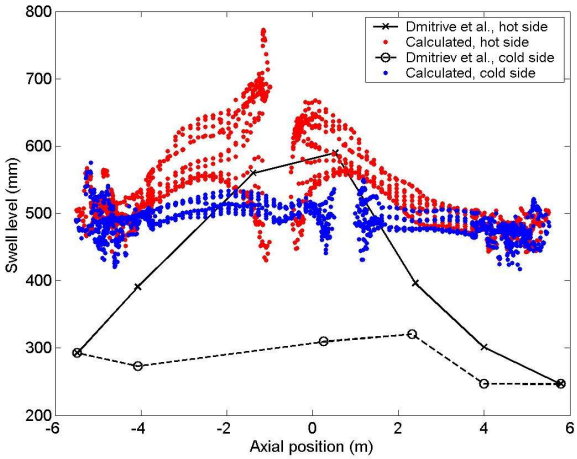

Fig. 10: Vertical position of the 70% mixture level on the hot and cold sides. The calculated vertical distance from the top of the tube banks is shown. In comparison, the swell level reported by Dmitriev et al. (1991) is shown.

Table 2: Comparison of the simulations to measured void fractions and flow velocities of liquid water. Simulation results obtained with the physical and superficial velocity formulations are shown.

	Void1 [-]	**Void2 [-]**	**Void3 [-]**	**Void4 [-]**	**Vel1 [m/s]**	**Vel2 [m/s]**	**Vel3 [m/s]**	**Vel4 [m/s]**
Measurement	0.3...0.4	0.3...0.4	0.3...0.4	0.3...0.4	0...0.4	0...0.4	0...0.4	0...0.4
Simulation, physical	0.31	0.42	0.31	0.30	0.31	0.30	0.07	0.26
Simulation, superficial	0.30	0.39	0.31	0.33	0.29	0.28	0.14	0.27

In Fig. 9, the velocity of liquid water is shown at the centre and in the hot end of the steam generator. In the gap between the tube banks and the shell, water flows downwards and the stagnation point is close to the centre of the steam generator or somewhat towards the hot side. On the hot side, water flows mainly upwards and on the cold side mainly downwards. This flow pattern is driven by the density difference caused by the different void fraction on the hot and cold sides.

4.2 Comparison with Available Measured Data

The available measured data on the secondary side of full size steam generators is very scarce. Only a few measurements for horizontal steam generators are known by the authors of the present report. We have chosen to compare the calculated void fractions and flow velocities to the measurements presented by Haapalehto and Bestion (1993). The four measurement points were located 70 cm below the top of the tube banks, and their positions are shown in Fig. 6.

In the porous media model of FLUENT 12.0, two alternative velocity formulations can be used: superficial and physical. In the superficial velocity formulation, the velocity in the porous region remains the same as outside the porous region, i.e., $v_{\text{superficial}} = \gamma v_{\text{physical}}$. The physical velocity model takes into account the acceleration of the flow in the region, where the flow area is reduced by the tubes. The physical velocity formulation has been used to obtain the results presented so far.

In Table 2, the calculated results are compared to measurements. Results obtained both with the physical and superficial velocity models are shown. The calculated void fractions are in a very good agreement with the measured values that were in the range 0.3...0.4 at all four measurement points. The error bars of the measured velocities of liquid water were unfortunately rather large: the flow velocities were 0...0.4 m/s. The calculated values fit well within this range.

Some information is also available on the position of the water surface in VVER-440 steam generators. Dmitriev et al. (1991) present the mixture level on the hot and cold sides of the steam generator. The exact definition of the measured "mixture level" is, however, not available. In Fig. 10,

we have plotted the calculated 70% mixture level together with the measured result. The qualitative similarity of the calculated and measured mixture level is apparent both on the hot and on the cold side. Quantitative comparison is hampered by the difficulty in the interpretation of the measured data.

5. SUMMARY AND DISCUSSION

A three-dimensional porous media model has been implemented for the secondary side of the horizontal steam generator of a VVER-440 plant by using the ANSYS FLUENT 12.0 code. The primary circuit is solved with the APROS system code and the outer wall temperatures are interpolated to the CFD model. Steady state operation at full power is solved.

The implemented model has been found to be robust and to converge well towards the stationary state, when time dependent simulations are performed. The calculated void fractions and flow velocities of liquid water are in good agreement with the measurements at the few measurement points, where measured data is available. The shape of the mixture level is in qualitative agreement with observations. More accurate measurements of void fractions, velocities and the mixture levels would be necessary for better validation of the model.

In general, the coarse mesh with 120 000 grid cells was found to produce very similar results as the finer mesh with 960 000 grid cells. The coarse mesh seems to be suitable for most practical applications. Some details of the solution, such as the jets of cold feed water, are not well captured by the coarse mesh. The wall friction is only properly resolved with the finer mesh. At least in steady state situations, this does not, however, affect too much the overall behaviour of the model.

Acknowledgement

This work has been done in the SAFIR2010 research programme (The Finnish Research Programme on Nuclear Power Plant Safety 2007–2010). The work has been funded by the Ministry of Employment and the Economy, VTT Technical Research Centre of Finland and Fortum Nuclear Services Ltd.

REFERENCES

ANSYS, ANSYS FLUENT 12.0 User's Guide, Ansys Inc., USA (2009).

APROS, Homepage of the APROS process simulation software, 20.4.2010, www.apros.fi (2010).

A.I. Dmitriev, Yu.v. Kozlov, S.S. Logvinov, G.A. Tarankov and V.F. Titov, "Separation characteristics of horizontal steam generators", OKB "Gidropress" International Seminar of Horizontal Steam Generator Modelling, vol. 1, LPR 1991.

T. Haapalehto and D. Bestion, "Horizontal steam generator modelling with CATHARE; validation of several nodalization schemes on plant data", CEN Grenoble, 2nd Int. Seminar on Horizontal Steam Generators (1993).

M. Ishii and N. Zuber, "Drag coefficient and relative velocity in bubbly, droplet and particulate flows", *AiChE Journal*, **25**, 843–855 (1979).

G. Kristóf, K.G. Szabó and T. Régert, "Modeling of boiling water flow in the horizontal steam generator of the Paks nuclear power plant", ANSYS Conference & 26th CADFEM Users' Meeting 2008, October 22–24, 2008, Darmstadt, Germany (2008).

Z.R. Simovic, S. Ocokoljic and V.D. Stevanovic, "Interfacial friction correlations for the two-phase flow across tube bundle", *Int. J. Multiphase Flow*, **33**, 217–226 (2007).

Z.V. Stosic and V.D. Stevanovic, "Advanced three-dimensional two-fluid porous media method for transient two-phase flow thermal-hydraulics in complex geometries", *Numer. Heat Transfer*, **B 41**, 263–289 (2002).